Macroscopic oscillations of a quadratic integrate-and-fire neuron network with global distributed-delay coupling

Irmantas Ratas and Kestutis Pyragas
Center for Physical Sciences and Technology, LT-10257 Vilnius, Lithuania

(Received 30 July 2018; published 26 November 2018)

We consider a large network of globally coupled quadratic integrate-and-fire neurons, which are canonical representatives for class I neurons near the spiking threshold. The model includes two heterogeneous parameters. One of them characterizes the state of isolated neurons and subdivides them into excitable and spiking units. The other heterogeneous parameter is the interaction delay time. In the infinite-size limit, we reduce the model to a simple system of ordinary differential equations. By bifurcation analysis of these equations, we identify the regions in the parameter space where the network exhibits macroscopic self-oscillations. The robustness of the oscillations against aging damage, which transforms spiking neurons into nonspiking neurons, is analyzed. We found an interesting counterintuitive effect when an increase in the proportion of nonspiking neurons induces macroscopic oscillations. The validity of the reduced equations is confirmed by comparing their solutions with the solutions of microscopic equations for a finite-size network. The solutions are compared not only for the periodic oscillation modes but also for the collective chaos regime.

DOI: 10.1103/PhysRevE.98.052224

I. INTRODUCTION

Studies of collective behavior in systems consisting of many coupled nonlinear dynamic units have been an active and continuing area of research in diverse fields ranging from physics to neuroscience [1–5]. An important early contribution in these studies was the introduction by Kuramoto [6] of a simple paradigmatic model for synchronization phenomena in large populations of interacting oscillators. The Kuramoto model describes a system of heterogeneous phase oscillators coupled to each other via sine function. The model was extensively studied during the past two decades [2–5]. A major breakthrough in these studies belongs to Ott and Antonsen [7]. Considering the thermodynamic limit, they reduced an infinite set of Kuramoto equations to a low-dimensional macroscopic model defined by a small system of ordinary differential equations (ODEs) for macroscopic order parameters. This approach, known as Ott-Antenson (OA) ansatz, stimulated the analysis of various modifications of the Kuramoto model [8–13]. Furthermore, OA ansatz was adopted for globally coupled networks of theta neurons [14–16], networks of theta neurons with spatially dependent coupling [17], networks incorporating gap junctions [18], and a pulse coupled Winfree model [19,20].

An alternative method to reduce microscopic equations of a particular class of neural systems has been proposed by Montbrió, Pazó, and Roxin [21]. The authors considered an infinite-size network of heterogeneous quadratic integrate-and-fire (QIF) neurons globally coupled via instantaneous pulses. They found that the corresponding continuity equation can be solved by a Lorentzian ansatz (LA) with two time-varying order parameters, which appeared to be biophysically relevant quantities, namely the mean membrane potential and the firing rate. As a result, the authors derived a simple system of two ODEs for these quantities. Although the LA and OA ansatz look quite different, there is a simple conformal mapping between their order parameters [21]. The LA has been successfully applied to various modifications of QIF neuron networks in subsequent publications [22–25]. In Ref. [22], the LA was extended to a more realistic synaptic coupling between QIF neurons by taking into account the finite width of synaptic pulses. Such a coupling resulted in more complex dynamics of the network, including the macroscopic self-oscillations of the mean field, which have not been observed in Ref. [21]. Another way to gain the macroscopic oscillations in the QIF neuron network has been demonstrated in Ref. [23]. Here, as well as in Ref. [21], the authors considered an interaction via instantaneous pulses but introduced a uniform delay in the coupling.

In this paper, we consider a network of QIF neurons with two heterogeneous parameters. One of them characterizes the state of isolated neurons in the network and the other is the interaction delay time. The introduction of heterogeneous interaction delays is motivated by the fact that in realistic neural networks axons have different lengths and are characterized by different transmission speeds, which leads to different signal transmission times between neurons [26,27]. We note that a more accurate model should include spatial coordinates and consider spike propagation between neurons. Here, as well as in Refs. [23], we consider a simplified model network of point neurons in which the spatial coordinates are ignored but the finite time of pulse propagation between neurons is taken into account using a communication delay. By employing the LA and the methods introduced in Ref. [28], we reduce the microscopic model to a finite set ($\geqslant 3$) of ODEs, which include three macroscopic variables, namely the mean membrane potential, the firing rate, and the mean synaptic current. Bifurcation analysis of these equations makes it possible to identify regions in the parameter space where macroscopic oscillations occur. We are mainly interested in the dependence of the oscillations on the heterogeneities of the network.

When studying large complex networks, an important practical problem is the robustness of network function under malfunctions of internal components. In this paper, we study the effect of aging, when local damages transform the spiking neurons into the nonspiking. When the proportion of inactive elements in a network exceeds some threshold value, the network ceases to generate macroscopic oscillations and its physiological function may be lost. Such a phenomenon is called an *aging transition*. Originally, the effect of aging transition was detected by Daido and Nakanishi [29] in two populations of coupled active and inactive Stuart-Landau oscillators. In Ref. [29], as well as in the subsequent publications [30–32], the elements in each of the subpopulations were identical. In more recent papers [22,33,34], the aging transition was analyzed in the case of one, but heterogeneous population in which both active and inactive elements are heterogeneous. In Refs. [35,36], an influence of heterogeneous interaction delay to aging transition were explored; however, the investigations were restricted to the case of two subpopulations with the identical elements in each of them. Here we consider a combined case, where both the network elements and the interaction delays are heterogeneous. We show that such a combination can cause a counterintuitive effect when an increase in the proportion of nonspiking neurons induces macroscopic oscillations in the network. Such *aging-induced oscillations* are opposed to the conventional aging transition.

The paper is organized as follows. In Sec. II, we describe our model and, in the infinite-size limit, derive the reduced macroscopic equations. Section III is devoted to the bifurcation analysis of the reduced equations. Then, in Sec. IV, we analyze the aging transition. In Sec. V, the solutions of the reduced macroscopic equations are compared with the results of direct numerical simulations of microscopic equations for a finite-size network. Finally, in Sec. VI we discuss the results.

II. MODEL DESCRIPTION

We consider a heterogeneous network of N all-to-all coupled quadratic integrate-and-fire neurons, which represent the canonical model for class I neurons near the spiking threshold. The microscopic state of the network is defined by the set of neurons' membrane potentials $\{V_i\}_{i=1..N}$, which satisfy the following equations:

$$\dot{V}_i = V_i^2 + \eta_i + JS_i(t). \tag{1}$$

Here η_i is a current that specify the behavior of each isolated neuron and the term $JS_i(t)$ defines the synaptic coupling between neurons, where J is the synaptic weight. For the uncoupled network, $J = 0$, the neurons with the negative value of the parameter $\eta_i < 0$ are quenched (they are in an excitable regime), while the neurons with the positive value of the parameter $\eta_i > 0$ generate instantaneous spikes, which are approximated by the Dirac delta function. The spikes are emitted at the moments when the membrane potential V_i reaches a peak value V_{peak}. Immediately after the spike emission the membrane potential is reset to V_{reset}. Thereafter, we take $V_{\text{peak}} = -V_{\text{reset}} \to \infty$. Then the interspike interval of the ith spiking neuron is $\text{ISI}_i = \pi/\sqrt{\eta_i}$. The heterogeneity of neurons is realized by spreading the values of the parameter η according to a distribution function $g(\eta)$, which will be specified below.

We consider a network of all-to-all time-delay coupled neurons. To this end, we incorporate link-dependent interaction time delays τ_{ji} for coupling between any two j and i neurons, so the mean synaptic current for the ith neuron is defined as

$$S_i(t) = \frac{1}{N}\sum_{j=1}^{N}\sum_{k\setminus t_j^k<t}\delta\left(t - t_j^k - \tau_{ji}\right), \tag{2}$$

where $\delta(t)$ is the Dirac delta function and t_j^k is the time of the kth spike of the jth neuron. We assume that the collection of all delays τ_{ji} is characterized by a distribution $h(\tau)$ such that the fraction of links with delays between τ and $\tau + d\tau$ is $h(\tau)d\tau$. We also assume that, for randomly chosen links, τ is uncorrelated with neuron parameters η at either end of the link. Thus, by spreading the time delay parameter, we introduce the second heterogeneity in the network, now in the coupling.

A. Thermodynamic limit $N \to \infty$

In the thermodynamic limit $N \to \infty$, the infinite-dimensional microscopic model (1) can be reduced to a finite-dimensional macroscopic model. To derive the macroscopic equations, we use the Lorentzian ansatz [21], which is closely related to the Ott-Antonsen ansatz [7,8]. Since the derivation is similar to that described in Refs. [7,21,28], here we present it in abbreviated form.

In the infinite-N limit, the macroscopic state of the system (1) can be described by a continuous density function $\rho(V|\eta,t)$. The product $\rho(V|\eta,t)dV$ defines the fraction of neurons with the membrane potential between V and $V + dV$ and parameter η at time t. Conservation of number of neurons implies that the density function $\rho(V|\eta,t)$ satisfies the continuity equation

$$\frac{\partial}{\partial t}\rho = -\frac{\partial}{\partial V}\{\rho[V^2 + \eta + JS(t)]\}. \tag{3}$$

For $N \to \infty$, the mean synaptic current (2) can be approximated by the integral

$$S(t) = \int_0^\infty r(t-\tau)h(\tau)d\tau, \tag{4}$$

where $r(t)$ is the total firing rate of neurons, i.e., the population-averaged number of spikes per unit time. The total firing rate is expressed through the integral $r(t) = \int_{-\infty}^{+\infty} r(\eta,t)g(\eta)d\eta$, where $r(\eta,t)$ is the firing rate of neurons with the fixed value of the parameter η. The latter is defined as the probability flux at $V \to +\infty$, i.e., $r(\eta,t) = \rho(V \to \infty|\eta,t)\dot{V}(V \to \infty|\eta,t)$.

According to Ref. [21], we look for a solution of Eq. (3) in the form of Lorentzian distribution

$$\rho(V|\eta,t) = \frac{1}{\pi}\frac{x(\eta,t)}{[V - y(\eta,t)]^2 + x(\eta,t)^2} \tag{5}$$

with time-dependent parameters $x(\eta,t)$ and $y(\eta,t)$ that define the half-width and the center of the distribution. These parameters are related to the total firing rate $r(t)$ and the mean

membrane potential $v(t)$ via integrals

$$r(t) = \frac{1}{\pi}\int_{-\infty}^{+\infty} x(\eta,t)g(\eta)d\eta, \tag{6a}$$

$$v(t) = \int_{-\infty}^{+\infty} y(\eta,t)g(\eta)d\eta. \tag{6b}$$

By substituting the LA Eq. (5) into the continuity equation (3), one can derive two differential equations for the parameters $x(\eta,t)$ and $y(\eta,t)$:

$$\dot{x}(\eta,t) = 2x(\eta,t)y(\eta,t), \tag{7a}$$

$$\dot{y}(\eta,t) = \eta - x^2(\eta,t) + y^2(\eta,t) + JS(t). \tag{7b}$$

It is assumed that all trajectories (for any initial conditions) of the system (3) reach the manifold (5) in a relatively short time, so all relevant dynamics of the system can be described in a reduced subspace and characterized by the evolution of the manifold parameters defined by Eqs. (7).

Further simplification can be achieved by a proper choice of the distribution functions for the heterogeneity parameters η and τ. Specifically, for the η parameter, we choose the Lorentzian distribution

$$g(\eta) = \frac{1}{\pi}\frac{\Delta}{(\eta-\bar{\eta})^2+\Delta^2}, \tag{8}$$

where $\bar{\eta}$ is the center of the distribution and Δ is its width. Such a choice allows us to solve the η integrals in Eqs. (6a) and (6b). This is performed by analytic continuation of $x(\eta,t)$ and $y(\eta,t)$ from real to the complex η plane and by the use of the residue theorem. As a result, the following expressions for the firing rate and the mean membrane potential are obtained: $r(t) = x(\bar{\eta}-i\Delta,t)/\pi$ and $v(t) = y(\bar{\eta}-i\Delta,t)$. By substituting these expressions into Eqs. (7), we obtain the following differential equations for these parameters:

$$\dot{r} = \Delta/\pi + 2rv, \tag{9a}$$

$$\dot{v} = \bar{\eta} + v^2 - \pi^2 r^2 + JS(t). \tag{9b}$$

Equations (9) together with Eq. (4) constitute the macroscopic model of the system. This model is significantly simpler than the microscopic model defined by Eqs. (1) and (2). However, in general, this model is still infinite dimensional, since it belongs to a class of differential equations with distributed delays. Nevertheless, the proper choice of the delay distribution function $h(\tau)$ allows us to reduce this system to a finite set of ordinary differential equations. As shown in Ref. [28], a convenient class of functions for this purpose is given by the gamma distribution

$$h(\tau) = \frac{A_n}{T^n}\tau^{n-1}\exp\left(-\frac{n\tau}{T}\right) \tag{10}$$

with a parameter n being a natural number, $n = 1, 2, \ldots$. Here T is the mean value of the distribution and $A_n = n^n/(n-1)!$ is a normalization parameter. The standard deviation of τ about its mean T is given by

$$\delta\tau = (\langle\tau^2\rangle - \langle\tau\rangle^2)^{1/2} = T/\sqrt{n}. \tag{11}$$

From here we see that the width of the distribution decreases with the increase of n and the distribution turns into the Dirac delta function $h(\tau) = \delta(\tau - T)$ when $n \to \infty$. The latter case corresponds to uniform delay, $\tau = T$, on all of the links. This case is previously considered in Ref. [23]. Here by varying n, we can study how the relative spread $\delta\tau/T$ in the delay times affects the dynamics of the network.

The gamma distribution enables the transformation of the convolution (4) into the differential equation for $S(t)$. Taking the Laplace transform of Eq. (4), we get

$$\hat{S}(s) = \hat{h}(s)\hat{r}(s), \tag{12}$$

where $\hat{S}(s)$ and $\hat{r}(s)$ are the Laplace transform of $S(t)$ and $r(t)$, respectively, and

$$\hat{h}(s) = \left(\frac{T}{n}s + 1\right)^{-n} \tag{13}$$

is the Laplace transform of the gamma distribution $h(\tau)$. Now dividing both sides of Eq. (12) by $\hat{h}(s)$ and transforming back to the time domain via substitution $s \to d/dt$, we get an nth-order differential equation for the mean synaptic current $S(t)$:

$$\left[\frac{T}{n}\frac{d}{dt} + 1\right]^n S(t) = r(t). \tag{14}$$

This equation can alternatively be rewritten in the form of a system of n first-order differential equations,

$$\frac{T}{n}\frac{dS_j}{dt} = S_{j+1} - S_j, \quad j = 1, \ldots, n, \tag{15}$$

for n variables $[S_1(t), \ldots, S_n(t)]$ and $S_{n+1}(t) = r(t)$. The first variable of this system defines the solution of Eq. (14), $S(t) = S_1(t)$. The form (15) is convenient for numerical simulations. Thus, for the given n, the macroscopic model of heterogeneous QIF neurons with the heterogeneous interaction delays is described by a system of $(n+2)$ ODEs consisting of Eqs. (9) and (15).

III. BIFURCATION ANALYSIS

In order to find the regions of the parameters where the system of coupled QIF neurons exhibits macroscopic oscillations, we look for local bifurcations of Eqs. (9) and (14). To this end, we analyze the linear stability of the equilibrium (fixed) points of the system. The system of Eqs. (9) and (14) is characterized by three dynamical variables: $r(t)$, $v(t)$, and $S(t)$. We denote the corresponding equilibrium values by overbars: $\bar{r}$, $\bar{v}$, and $\bar{S}$. They are found from Eqs. (9) and (14) by equating the derivatives of the variables to zero. From Eq. (14) it follows that $\bar{S} = \bar{r}$. Then by substituting this relation into Eqs. (9) and equating their right-hand sides to zero, we obtain equations for the equilibrium values of $\bar{r}$ and $\bar{v}$:

$$\Delta/\pi + 2\bar{r}\bar{v} = 0, \tag{16a}$$

$$\bar{\eta} + \bar{v}^2 - \pi^2\bar{r}^2 + J\bar{r} = 0. \tag{16b}$$

From these equations, we see that the equilibrium values are independent of the parameters n and T of the delay distribution function $h(\tau)$. They depend only on the parameters Δ and $\bar{\eta}$ of the distribution function $g(\eta)$ as well as the coupling strength J. However, we emphasize that the stability of equilibrium points depends on all the above parameters.

Here we restrict our analysis to the case $\bar{\eta} > 0$, when most of uncoupled QIF neurons are spiking. Then Eqs. (16) has a single solution, i.e., the system possesses a single fixed point. Although the coordinates of this fixed point cannot be written explicitly, the bifurcation curves in different planes of the system parameters can be derived in a parametric form.

In order to analyze the linear stability of the fixed point, we substitute $r = \bar{r} + \delta r$, $v = \bar{v} + \delta v$, and $S = \bar{S} + \delta S$ into Eqs. (9) and (14) and linearize them with respect to small deviations $(\delta r, \delta v, \delta S)$. Then by looking for the solution of the linearized equations in the form $(\delta r, \delta v, \delta S) \propto \exp(\lambda t)$, we obtain the characteristic equation

$$[(2\bar{v} - \lambda)^2 + 4\bar{r}^2\pi^2](1 + \lambda T/n)^n - 2J\bar{r} = 0 \tag{17}$$

that defines the eigenvalues λ of the fixed point. Equation (17) is an $(n+2)$-order polynomial equation with respect to λ and thus it has $(n+2)$ roots. The fixed point is stable if the real parts of all roots are negative and is unstable if the real part of at least one root is positive.

A. Andronov-Hopf bifurcation

Andronov-Hopf (AH) bifurcation is a local bifurcation that defines the birth of a limit cycle from an equilibrium, when the equilibrium changes stability. This happens when two leading complex conjugate eigenvalues simultaneously cross the imaginary axis of the complex plane. By leading eigenvalues we mean the eigenvalues with the maximum real part. Thus, at the AH bifurcation point there exists a purely imaginary eigenvalue $\lambda = i\omega$ that satisfies Eq. (17):

$$[(2\bar{v} - i\omega)^2 + 4\bar{r}^2\pi^2](1 + i\omega T/n)^n - 2J\bar{r} = 0. \tag{18}$$

Here ω is a real parameter referred to as a Hopf frequency. All the AH bifurcation points satisfy Eqs. (16) and (18). However, not all solutions of Eqs. (16) and (18) correspond to the AH bifurcation points, since these equations are also satisfied when nonleading eigenvalues cross the imaginary axis. In order to identify the right AH bifurcation points in the parameter space, we have to select only those solutions of Eqs. (16) and (18) for which all other roots of Eq. (17) have negative real parts, $\mathrm{Re}(\lambda) < 0$.

Equations (16) and (18) are very convenient to construct the AH bifurcation curves in some two-dimensional projections of the parameter space. It appears that the solutions of these equations can be presented in a parametric form. Below we demonstrate such a construction of the AH bifurcation curves in (T, J) and (Δ, J) parameter planes.

1. (T, J) plane

First, we assume that all parameters of the system are fixed except for the parameters T and J and derive parametric equations for the AH bifurcation curves in the (T, J) plane. To this end, we introduce a parameter

$$q = \omega T/n \tag{19}$$

and treat it as an independent variable. We seek to present the solutions of Eqs. (16) and (18) in the parametric form $T = T(q)$ and $J = J(q)$. Let us denote $(1 + iq)^n \equiv A(q) + iB(q)$ and insert this definition into Eq. (18). Then by separating the real and imaginary parts, we get

$$[4\bar{v}^2 - \omega^2 + 4\pi^2\bar{r}^2]A + 4\bar{v}\omega B = 2J\bar{r}, \tag{20a}$$

$$[4\bar{v}^2 - \omega^2 + 4\pi^2\bar{r}^2]B - 4\bar{v}\omega A = 0. \tag{20b}$$

After some manipulations with the Eqs. (16) and (20), we get a polynomial equation for $\bar{r}$

$$C_8\bar{r}^8 + C_6\bar{r}^6 + C_4\bar{r}^4 + C_2\bar{r}^2 + C_0 = 0, \tag{21}$$

where C_j are the following coefficients:

$$C_8 = 4B^2\pi^4, \tag{22a}$$

$$C_6 = -8B^2\bar{\eta}\pi^2, \tag{22b}$$

$$C_4 = 2[4A\Delta^2 R - 8\Delta^2 R^2 - (\Delta^2 - 2\bar{\eta}^2)B^2], \tag{22c}$$

$$C_2 = 2\bar{\eta}\Delta^2[B^2 - 4AR]/\pi^2, \tag{22d}$$

$$C_0 = \Delta^4[B^2 - 16R^2 - 8AR]/4\pi^4. \tag{22e}$$

Here we introduced a notation $R = A^2 + B^2$. Since the parameters A and B are functions of q, the parameter R as well as the parameters C_j of the polynomial Eq. (21) are also functions of q. Thus, by solving this equation, we obtain $\bar{r}$ as a function of q, $\bar{r} = \bar{r}(q)$. Then from Eq. (16a), we get $\bar{v}(q) = -\Delta/2\pi\bar{r}(q)$ and from Eq. (16b) obtain

$$J(q) = [\pi^2\bar{r}^2(q) - \bar{v}^2(q) - \bar{\eta}]/\bar{r}(q). \tag{23}$$

Next, from Eqs. (20), we derive the dependence of the Hopf frequency ω on q, $\omega(q) = \bar{r}(q)/2\bar{v}(q)R(q)$, and from Eq. (19) finally get

$$T(q) = nq/\omega(q). \tag{24}$$

Examples of using the parametric Eqs. (23) and (24) are presented in Fig. 1. Here we plot the AH bifurcation curves in (T, J) plane for the fixed $\bar{\eta} = 1$ and different fixed values of the parameters Δ and n that define the widths of the distribution functions $g(\eta)$ and $h(\tau)$, respectively. The colored areas show the regions of the parameters where the equilibrium is unstable and thus the oscillations of the firing rate and the mean membrane potential take place. The left column in the figure corresponds to the homogeneous neurons ($\Delta = 0$). The relative spread of interaction delays increases from bottom to top (n is decreased from 16 to 4). When the interaction delays are scattered modestly ($n = 16$), the macroscopic oscillations appear in stripelike areas of the (T, J) plane (see the bottom-left graph in the figure). The oscillations appear for both the inhibitory ($J < 0$) and excitatory ($J > 0$) couplings. The stripes are more pronounced for the excitatory coupling. If we fix the coupling strength J at some positive value and vary the mean value T of the delay time, we identify alternating intervals of T with and without macroscopic oscillations. The inhibitory coupling, $J < 0$, is more favorable for macroscopic oscillations, since for $J < 0$ the colored area is larger than that for $J > 0$. From the top left graph, we see that the excitatory coupling can also be favorable for macroscopic oscillations provided that the width of the delay distribution function is sufficiently large ($n = 4$). Here the colored areas for $J > 0$ and $J < 0$ are comparable.

In Fig. 1, the middle and the left columns show an influence of the heterogeneity of neurons. When the interaction delays

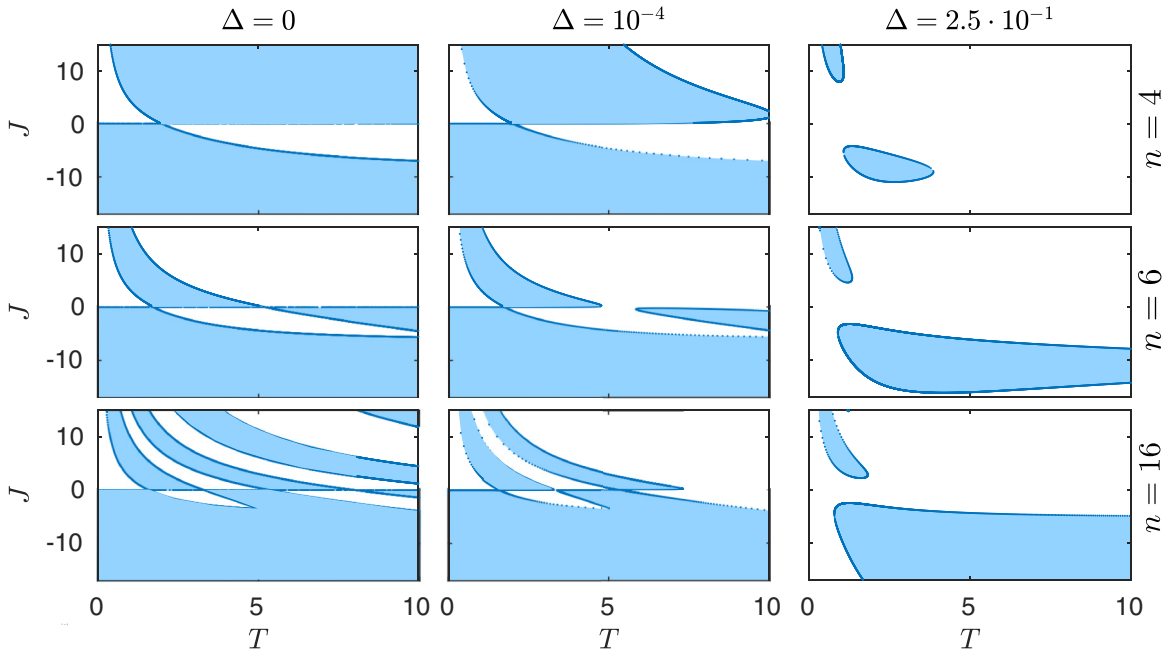

FIG. 1. Andronov-Hopf bifurcation diagrams of the macroscopic model Eqs. (9) and (14) in the (T, J) parameter plane. The points are estimated from the parametric Eqs. (23) and (24). The colored regions show where the equilibrium is unstable. Parameters: $\bar{\eta} = 1$, the columns correspond to $\Delta = 0, 10^{-4}, 2.5 \times 10^{-1}$ from left to right, and the rows correspond to $n = 4, 6, 16$ from top to bottom, respectively.

are weakly scattered, the system is very sensitive to a small heterogeneity of neurons. This is evident from the bottom row of the figure ($n = 16$). A little increase of the width Δ of the distribution function $g(\eta)$ from 0 to the value 10^{-4} drastically reduces the number and the sizes of the colored areas. In the right column ($\Delta = 0.25$), only two colored areas corresponding to the macroscopic oscillations remain. The sizes of these areas rapidly reduce with the increase of the width of the delay distribution function (top right graph). Thus the macroscopic oscillations do not appear in the neural network if both the parameters η and τ are strongly heterogeneous.

2. (Δ, J) plane

In order to construct the AH bifurcation curves in the (Δ, J) plane, we choose ω as an independent variable and look for the solutions of Eqs. (16) and (18) in the parametric form $\Delta = \Delta(\omega)$ and $J = J(\omega)$. Similarly as in Sec. III A 1, we denote $(1 + i\omega T/n)^{n+1} \equiv A(\omega) + iB(\omega)$. The parameters A and B satisfy the same Eqs. (20b), but unlike in Sec. III A 1, now they are functions of the variable ω rather than q. By performing mathematical operations with Eqs. (16) and (20), we find that the potential $\bar{v}$ satisfies the quadratic equation

$$4B\bar{v}^2 + 2(2R - A)\omega\bar{v} + B(2\bar{\eta} - \omega^2/2) = 0. \tag{25}$$

By solving this equation, we obtain $\bar{v}$ as a function of ω, $\bar{v} = \bar{v}(\omega)$. Then from Eq. (20b), we define $\bar{r}$ as a function of ω, $\bar{r}(\omega) = [\omega\bar{v}(\omega)A(\omega)/B(\omega) + \omega^2 - \bar{v}^2(\omega)]^{1/2}/\pi$ and, finally, from Eqs. (16) derive the parametric equations:

$$\Delta(\omega) = -2\pi\bar{r}(\omega)\bar{v}(\omega), \tag{26a}$$

$$J(\omega) = \pi^2\,\bar{r}(\omega) - [\bar{\eta} + \bar{v}^2(\omega)]/\bar{r}(\omega). \tag{26b}$$

In Fig. 2, we draw the AH bifurcation curves in the (Δ, J) plane for the fixed $\bar{\eta} = 1$ and different fixed values of the parameters T and n that define the mean and the relative width $\delta\tau/T = 1/\sqrt{n}$ of the distribution function $h(\tau)$, respectively. The relative width of the delay distribution decreases in columns from left to right. We see that macroscopic oscillations persist for higher diversity (larger Δ) of neurons the smaller is the scatter of delays (the larger n). Nevertheless, for any fixed n there exists a threshold value of Δ beyond which the macroscopic oscillations disappear. Again, we see that the inhibitory coupling is more favorable for macroscopic oscillations. An exceptional case is the top left graph ($n = 4$ and $T = 1$), where the oscillating areas for the inhibitory ($J < 0$) and excitatory ($J > 0$) couplings are comparable. The increase of the mean delay T (see the rows in the figure from top to bottom) decreases the lengths and the widths of oscillating regions for the excitatory coupling. For the inhibitory coupling, there exists only one oscillating region and its size is almost independent of the parameters T and n of the delay distribution function.

IV. AGING TRANSITION

In the studies of complex neural networks, an important problem is the robustness of network structure and function under external perturbations. Of particular interest is the question of how robust is macroscopic activity of a network against local damages that convert spiking neurons into nonspiking neurons. When the proportion p of the inactive neurons is increased, the amplitude of global oscillations decreases and vanishes at some critical value p_c. This phenomenon is called the aging transition. The parameter p_c varies in the interval [0,1] and serves as a measure for the robustness against aging. For a network of QIF neurons, coupled globally via synaptic

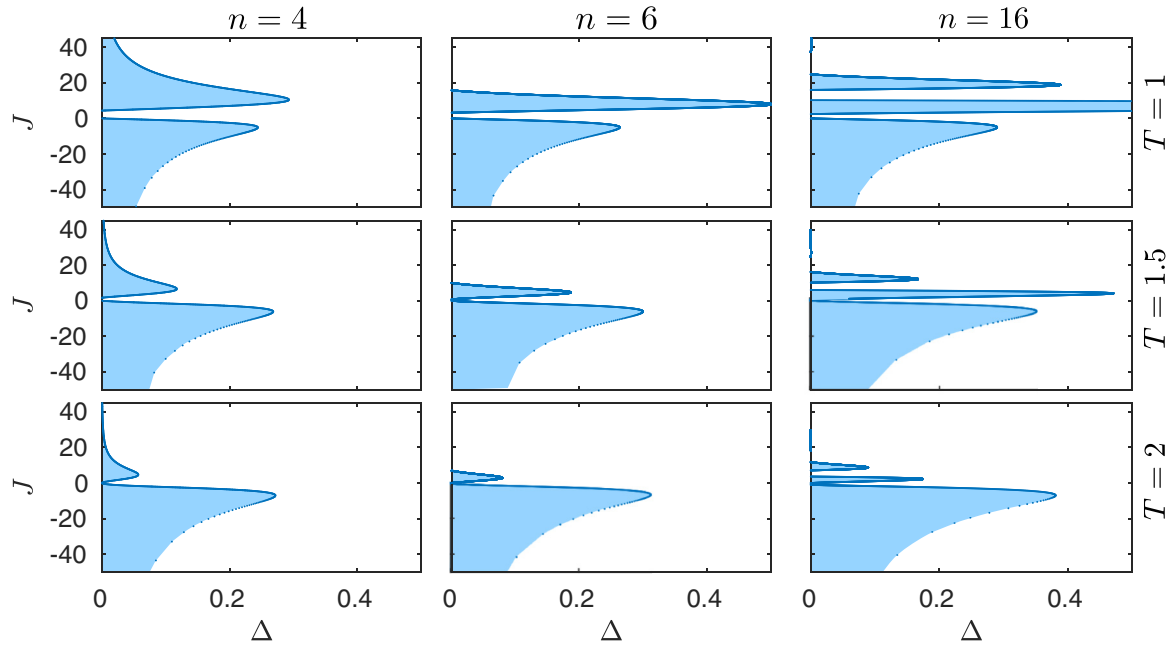

FIG. 2. Andronov-Hopf bifurcation diagrams of the macroscopic model Eqs. (9) and (14) in (Δ, J) parameter plane. The points are estimated from the parametric Eqs. (26). The colored regions show where the equilibrium is unstable. Parameters: $\bar{\eta} = 1$, the columns correspond to $n = 4, 6, 16$ from left to right, and the rows correspond to $T = 1, 1.5, 2$ from top to bottom, respectively.

pulses of finite width, the aging transition was considered in Ref. [22]. It has been shown that the network is highly robust against aging damage if the synaptic pulses are sufficiently wide and high. However, the influence of time delays in the interactions between neurons has not been considered. Here we investigate the same problem, assuming that the interaction between neurons is provided by instantaneous pulses with distributed delays. We show that the presence of delays in the interaction considerably complicates the scenario of the aging transition.

Our analysis of the aging transition is based on the macroscopic model defined by Eqs. (9) and (14). We are particularly interested in how the aging transition depends on the coupling strength J, the width $\delta\tau$, and the mean delay T of the delay distribution function $h(\tau)$. In our model, the parameter η subdivides the neurons into spiking and nonspiking ones. The isolated ($J = 0$) neurons with the parameter $\eta > 0$ are spiking, while the neurons with the parameter $\eta < 0$ are nonspiking. The parameter η is distributed according to the Lorentz function (8), so the proportion of inactive neurons in the uncoupled network is

$$p = \frac{1}{2} - \frac{1}{\pi}\arctan(\bar{\eta}/\Delta). \tag{27}$$

In the following, we assume that the parameter Δ is fixed. Then the proportion of inactive neurons is uniquely defined by the center $\bar{\eta}$ of Lorentz distribution (8). The proportion p monotonically decreases from 1 to 0 when the center $\bar{\eta}$ of the distribution moves from $-\infty$ to $+\infty$ and crosses the value $p = 1/2$ at $\bar{\eta} = 0$.

In Fig. 3, we present the bifurcation diagram in the (p, J) parameter plane. The black dots represent the saddle-node (SN) bifurcation. As pointed out in Sec. III, the introduced delays affect only the stability of the equilibrium points, but do not change their number and positions. This fact allows us to find the SN bifurcation parametrically, in a similar way as described in Ref. [21]. The red and blue dots show the supercritical and subcritical AH bifurcations, respectively. These points are estimated from the the parametric equations $J = J(\omega)$ and $\bar{\eta} = \bar{\eta}(\omega)$, which we derive from Eqs. (16) and (18). First from Eq. (16a) we find the relation $\bar{v} = -\Delta/2\pi\bar{r}$. Inserting this relation into Eq. (20b), we arrive at the fourth

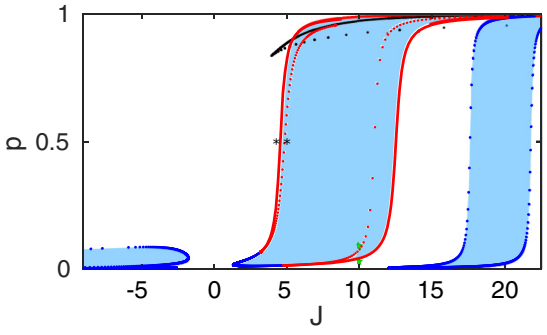

FIG. 3. Aging transition: the bifurcation diagram in the (J, p) plane. The black dots represent the saddle-node bifurcation. The red and blue dots show the supercritical and subcritical AH bifurcations, respectively. The red solid curve indicates the limit point of cycles bifurcation. The colored regions correspond to macroscopic oscillations of the firing rate and the mean membrane potential. The regions between red points and red solid curves correspond to bistability. Here the stable equilibrium and the stable limit cycle coexist. The two black asterisks at $p = 0.5$ and two green stars at $J = 10$ denote the values of the parameters at which the dynamics of the system are demonstrated in the subsequent figures. Parameters: $n = 16$, $T = 1$, and $\Delta = 0.25$.

order polynomial equation for the variable $\bar{r}$,

$$4B\pi^4\bar{r}^4 - B\omega^2\pi^2\bar{r}^2 + 2\Delta\omega A\pi\bar{r} + B\Delta^2 = 0. \qquad (28)$$

In this equation, the coefficients A and B are functions of ω, similarly as in Sec. III A 2. By solving this equation, we get $\bar{r}$ as a function of ω. Finally, from Eqs. (20a) and (16b), we obtain the desired parametric equations by expressing J and $\bar{\eta}$ as functions of ω. The red solid curve indicates the limit point of cycles bifurcation, where two limit cycles, one stable and other unstable, collide and disappear. This curve is obtained by numerical continuation [37]. The colored regions correspond to the presence of macroscopic oscillations and the borders of these regions define the dependence of the robustness parameter p_c on the coupling strength J. In the regions between red points and red solid curves the system is bistable. Here, depending on the initial conditions, the system approaches either the stable equilibrium or the stable limit cycle.

There are four important things to notice in Fig. 3. First, the inhibitory coupling is sensitive (not robust) to the aging damage. The oscillations in the region $J < 0$ exist only when a small proportion of neurons in the network are inactive. This is despite the fact that the inhibitory coupling is robust to the variation of the heterogeneity parameters n, T, and Δ (see Figs. 1 and 2).

Second, for the excitatory coupling, the aging transition has a resonance-like structure in the dependence of the coupling strength $J > 0$. The oscillating and nonoscillating regions alternate when the coupling strength is increased.

Third, in the oscillating regions, the network is robust to the aging damage. In these regions, the oscillations exist almost for any values of p. The network is able to preserve the mean field oscillations even when the proportion of inactive neurons is close to one. This is despite the fact that the excitatory coupling is sensitive to the variation of the heterogeneity parameters n, T, and Δ (see Figs. 1 and 2).

Fourth, for some values of the coupling strength, the presence of nonspiking neurons is necessary to gain macroscopic oscillations. For example, for fixed $J = 10$, the oscillations appear when the proportion p of inactive neurons exceeds some critical nonzero value $p_c = 0.043$. For $p < p_c$, there are no oscillations. The dynamics of the spiking rate derived from the macroscopic model for $p = 0.04 < p_c$ and $p = 0.075 > p_c$ are shown in Figs. 4(a) and 4(b), respectively. This is the most striking feature of the aging transition caused by the delays in the interaction. In contrast to the conventional aging transition, here an increase in the proportion of inactive neurons leads to the macroscopic oscillations of the network. Such *aging-induced oscillations* have not been observed in Ref. [22], where the similar network was analyzed without taking into account interaction delays.

The dependence of the AH bifurcation diagram in the (J, p) plane on the width of the delay distribution function (10) is shown in Fig. 5. We see that the effect of aging-induced oscillations is more pronounced with a large spread of delays. For $n = 5$ (top graph), there is the only oscillation region, which is raised above the J axis. When n is increased (middle graph), an additional oscillating region appears, which is very close to the J axis. Finally, for the uniform delay $n = \infty$ (bottom graph), the oscillation region touches the J axis, and, therefore, the effect of aging-induced oscillations disappears.

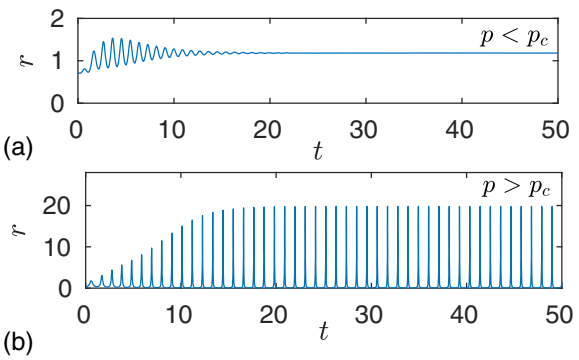

FIG. 4. Demonstration of aging-induced oscillations. The dynamics of the spiking rate derived from the macroscopic model Eqs. (9) and (15) at $n = 16$, $T = 1$, $\Delta = 0.25$, and $J = 10$. (a) The macroscopic oscillations do not appear if the proportion of inactive neurons is too small, $p = 0.04 < p_c = 0.043$. (b) Whenever the proportion of inactive neurons exceeds the critical value $p = 0.075 > p_c$, the network starts to generate macroscopic oscillations. The values of the parameters used here are marked by green stars in Fig. 3.

In order to explore the resonance-like structure of the aging transition shown in Fig. 3 in more detail, we fix the proportion of nonactive neurons at $p = 0.5$ and analyze how the number and the widths of the oscillating regions depend on the parameters of the delay distribution function $h(\tau)$. The results are presented in Fig. 6, where the AH bifurcation diagrams are shown in the plane of the parameters $(J, \delta\tau/T)$ for different values of the mean delay time T. The relative spread

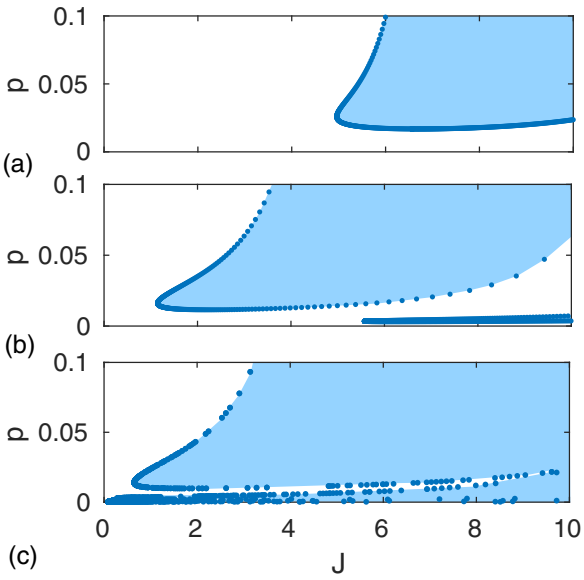

FIG. 5. The dependence of the AH bifurcation diagram in the (J, p) plane on the width of the delay distribution function (10): (a) $n = 5$, (b) $n = 20$, and (c) $n = \infty$. The parameters $T = 1$ and $\Delta = 0.25$ are the same as in Fig. 3. Colored areas correspond to unstable equilibrium where macroscopic oscillations occur.

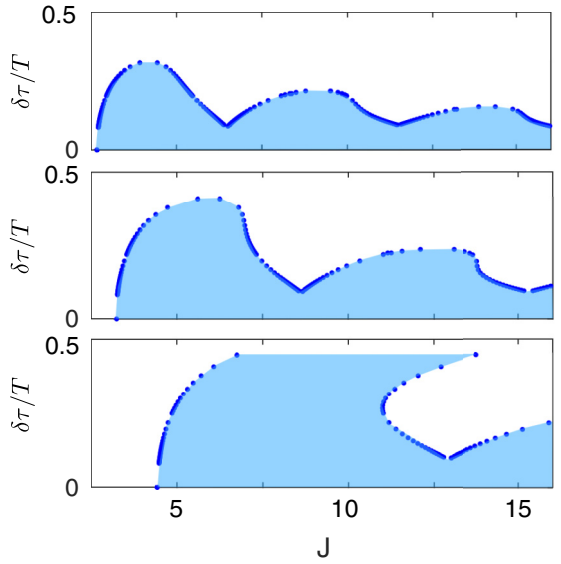

FIG. 6. The AH bifurcation diagrams in the plane $(J, \delta\tau/T)$ for the fixed proportion $p = 0.5$ ($\bar{\eta} = 0$) of inactive neurons and different values of the mean delay time, from top to bottom: $T = 2$, $T = 1.5$, and $T = 1$.

$\delta\tau/T = 1/\sqrt{n}$ of the delay distribution function were changed by varying the parameter n. By intersecting these diagrams with the horizontal line $\delta\tau/T = \text{const}$, we can identify the number and the widths of the oscillating intervals in the coupling strength J for any given $\delta\tau/T$. We see that oscillations do not appear if the relative spread $\delta\tau/T$ in the delay times is large. By gradually decreasing $\delta\tau/T$, first one oscillating region in the coupling strength J appears and broadens. Then further decrease of $\delta\tau/T$ leads to the appearance of the second, third, and so on, regions. The larger the mean delay time T, the more regions appear. All these regions broaden with the decrease of $\delta\tau/T$ and at some critical value all the regions merge together. For small-enough $\delta\tau/T$, the oscillations exist at any $J > J_c$, where J_c is a threshold value. The threshold J_c depends on the mean delay time T. The larger T, the smaller is the threshold J_c.

V. NUMERICAL SIMULATIONS

The reduced macroscopic Eqs. (9) and (15) are derived in the limit of an infinite-size network, while realistic networks consist of a finite number of neurons. In order to verify how well the macroscopic model predicts the behavior of a finite-size network, in Figs. 7 and 8 we compare the solutions of the macroscopic Eqs. (9) and (15) with the solutions of the microscopic model Eqs. (1) and (2). In both figures, the networks are composed of $N = 5000$ QIF neurons with the same values of the parameters $\bar{\eta} = 0$, $\Delta = 0.25$, $T = 1$, $n = 16$ and different values of the coupling strength J, which is equal to 4.5 and 5 in Figs. 7 and 8, respectively. The top graphs shows the spiking rate dynamics. The red dashed curves represent the solutions of the macroscopic Eqs. (9) and (14), while the blue solid curves show the microscopic dynamics of Eqs. (1) and (2). The bottom graphs represent

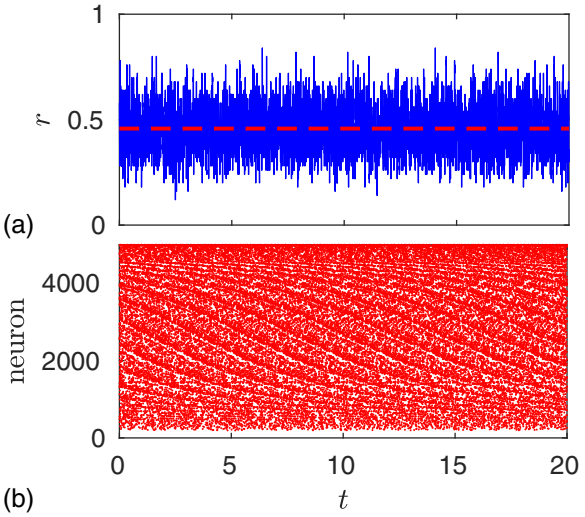

FIG. 7. (a) Comparison of the dynamics of the spiking rate estimated from the microscopic model Eqs. (1) and (2) (blue solid curve) and the reduced macroscopic model Eqs. (9) and (15) (red dashed curve). The results of the microscopic model are smoothed by using a moving average with a time window of the size 10^{-2}. (b) Spike raster plot. Dots correspond to firing events of individual neurons derived from the microscopic model. The network consist of $N = 5000$ quadratic integrate and fire neurons with the parameters $\bar{\eta} = 0$, $\Delta = 0.25$, $T = 1$, $n = 16$, and $J = 4.5$. The values of the parameters used here are marked by left black asterisk in Fig. 3. The Lorentzian distribution Eq. (8) were deterministically generated using $\eta_j = \bar{\eta} + \Delta \tan[(\pi/2)(2j - N - 1)/(N + 1)]$, $j = 1, \ldots, N$. For details of numerical simulation of the microscopic model see Ref. [22].

the spike raster plots, where dots indicate the firing events of individual neurons obtained from the microscopic model.

Figure 7 corresponds to the stable equilibrium. According to the macroscopic model, the spiking rate is constant; it is shown by the horizontal red dashed line. The spiking rate obtained from the microscopic model (blue solid curve) fluctuates around this predicted value. The fluctuations occur

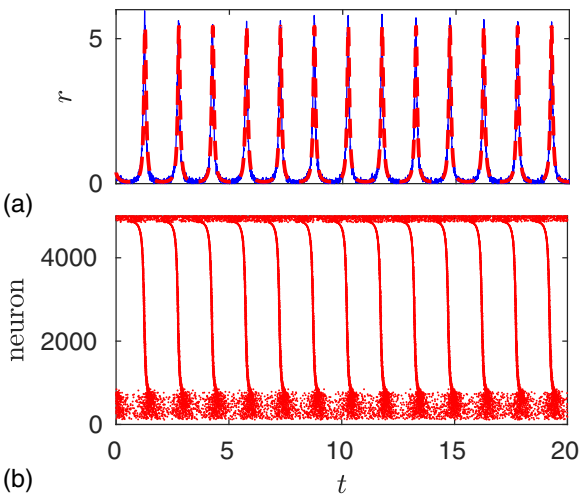

FIG. 8. The same as in Fig. 7, but for the coupling strength $J = 5$. The values of the parameters used here are marked by right black asterisks in Fig. 3.

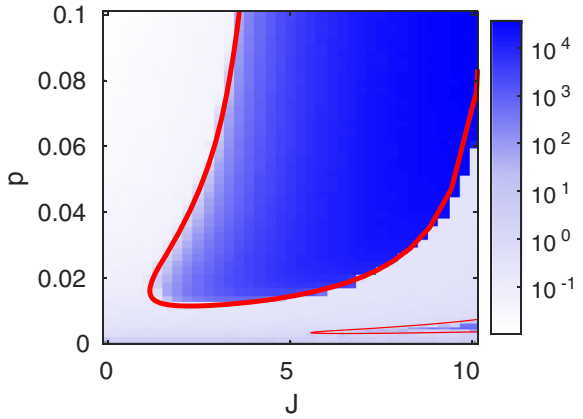

FIG. 9. Comparison of the color plot of the variance of the mean membrane potential, estimated by a microscopic model, with the AH bifurcation diagram in the (J, p) plane presented in Fig. 5(b). When estimating the mean membrane potential, the contribution from neurons with extremely large values of the membrane potential, $V_j > 500$, was ignored. This allowed us to avoid the divergence of this parameter. The red solid lines show the AH bifurcation curves. The number of neurons in the network is $N = 2000$. Other parameters are the same as in Fig. 5(b).

due to the finite size of the network. The neurons in this case produce uncorrelated spikes as is evident from the spike raster plot. Figure 8 demonstrates the regime of periodic macroscopic oscillations. Now the raster plot shows highly correlated spikes of the neurons. The spiking rate dynamics estimated from the microscopic model is in excellent agreement with that obtained from the macroscopic model. This confirms the validity of the derived macroscopic Eqs. (9) and (15).

The ability of a macroscopic model to predict the behavior of a finite size network is further demonstrated in Fig. 9. Here we present a color plot of a synchronization measure in the (J, p) plane and compare it with the bifurcation diagram presented in Fig. 5(b). As a measure of synchronization, we choose the variance of the mean membrane potential. Small values of this parameter correspond to a stable equilibrium of the network, while large values indicate macroscopic oscillations. We see that the AH bifurcation curves, obtained from the macroscopic model, correctly predict the oscillation regions in the (J, p) plane.

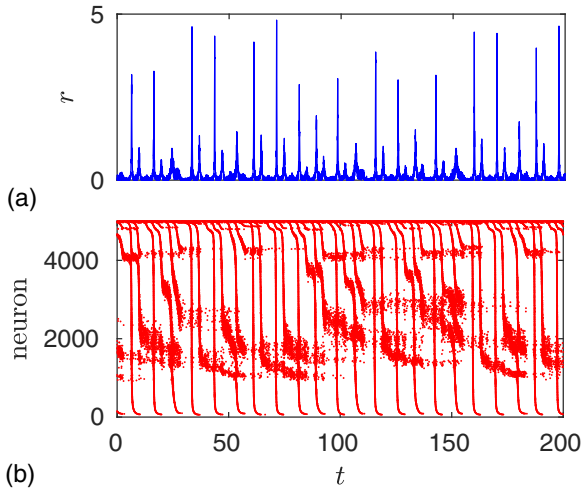

FIG. 10. Example of the collective chaos obtained by simulation of microscopic Eqs. (1) and (2): (a) spiking rate and (b) spike raster plot. Parameters: $N = 5000$, $J = -5.5$, $\bar{\eta} = 1$, $\Delta = 0.025$, $T = 3.5$, and $n = 101$ ($\delta\tau/T \approx 0.1$).

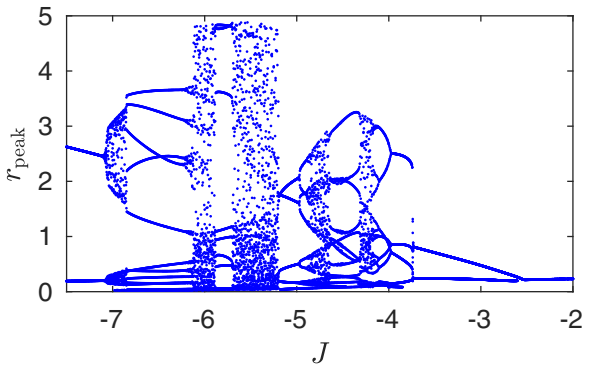

FIG. 11. One-parameter bifurcation diagram derived from the macroscopic model Eqs. (9) and (15). The peak values of the spiking rate are shown as functions of a smoothly varying coupling strength J. Parameters: $\bar{\eta} = 1$, $\Delta = 0.025$, $T = 3.5$, and $n = 101$ ($\delta\tau/T \approx 0.1$).

In a recent publication, Pazó and Montbrió [23] have shown that collective chaos can emerge in a population of identical inhibitory neurons with the uniform delayed coupling. Their consideration corresponds to the special case of our model, when $\Delta = 0$ and $n \to \infty$. The authors of Ref. [23] also analyzed the robustness of the chaotic state with respect to weak heterogeneities of neurons. They ascertained that collective chaos persists for small nonzero Δ, however, they did not consider the influence of the spread in the delay times. In Fig. 10, we show that collective chaos is present in the microscopic model Eqs. (1) and (2) when both heterogeneities, in the neurons and in the interaction delays, are taken into account. Scenarios of transition to chaos can be identified by analysis of the macroscopic model Eqs. (9) and (15). In Fig. 11, we plot the peak values r_{peak} of the spiking rate as functions of a smoothly varying coupling strength J. We see that with the decrease of J, chaos appears through a period doubling bifurcation, which starts at $J \approx -2.6$. When increasing J, chaos appears through quasiperiodic oscillations, which start at $J \approx -7.12$. The numerical analysis of the macroscopic model shows that chaotic regimes are very sensitive to small variations of the parameters Δ and n that define the widths of $g(\eta)$ and $h(\tau)$ distribution functions, respectively.

VI. DISCUSSION

In this paper, we analyzed the dynamics of heterogeneous network of quadratic integrate-and-fire neurons with global distributed-delay coupling. The network is composed of a mixture of excitable and spontaneously spiking neurons that emit instantaneous pulses. The heterogeneity of neurons is provided by spreading the neuron's current parameter η via

the Lorentz density function, while the heterogeneity in the interaction delay time τ is defined by the gamma distribution. By using a recently developed reduction technique based on the Lorentzian ansatz [21], we derived a closed system of ordinary differential equations for three macroscopic variables, namely, the mean membrane potential, the spiking rate and the mean synaptic current. The derived macroscopic equations are exact in the limit of an infinite-size network.

In order to identify the regions of the system parameters, where the network exhibits macroscopic self-oscillations, we performed the bifurcation analysis of the system. We showed that the interaction delays do not affect the number and the position of the equilibrium points but influence only their stability. We derived parametric equations for the Andronov-Hopf bifurcation curves that allowed us to identify the regions of the macroscopic oscillations in different two-dimensional projections of the parameter space. The main result of this analysis is that the macroscopic oscillations can only exist when the spreads of both heterogeneity parameters η and τ are sufficiently small.

We also analyzed an influence of interaction delays on the aging transition. The aging transition characterizes the robustness of the macroscopic self-oscillations against damage that increases the proportion p of inactive neurons in the network. When this proportion is increased to some critical value p_c, the network loses its oscillatory dynamics. The analysis of the aging transition in a similar network of QIF neurons, but interacting without delay, has been performed in Ref. [22]. Here we show that the interaction delays considerably complicate the phenomenon of the aging transition. Because of the delays, the aging transition has a resonance-like structure in the dependence of the coupling strength. More importantly, we revealed a striking feature that contradicts with the conventional definition of the aging transition. In some parameter regions, we found out that the presence of nonspiking neurons is necessary to gain macroscopic oscillations, i.e., the oscillations appear only when the proportion p of inactive neurons exceeds some critical nonzero value p_c, while for $p < p_c$ there are no oscillations. Such *aging-induced oscillations* are counterintuitive and, to our best knowledge, they have not been observed in previous studies of the aging transition. Here we found this effect for the QIF neuron network. An interesting question for further research is whether the effect will remain when replacing QIF neurons with another type of neurons.

Although the macroscopic equations are derived in the thermodynamic limit of an infinite number of neurons, they are well suited to predict the behavior of realistic, finite-size networks. We compared the solutions of the macroscopic equations with the numerical simulations of the microscopic model. For a network consisting of 5000 QIF neurons, we got an excellent agreement between the above two solutions. In addition, by numerical analysis of the macroscopic equations in different parameter regions, we found the collective chaos regime and confirmed its existence by direct numerical simulation of the microscopic model.

Macroscopic models of the type considered here are universal in the sense that they describe a network of canonical class I neurons, which are modeled by the equation of the normal form, universal near the spiking threshold. Such models can be considered as an alternative [38] to the phenomenological neural mass models [39], which are useful for understanding brain rhythms. The advantage of the macroscopic model considered here is that it describes exactly an underlying microscopic dynamics of the system. In this context, further development of this model is desirable. A practically important problem is the derivation of the macroscopic equations for more complex networks, where the coupling is not global but is rather determined by a specific network topology.

ACKNOWLEDGMENTS

This work was supported by Grant No. S-MIP-17-55 of the Research Council of Lithuania.

[1] A. Pikovsky, M. Rosenblum, and J. Kurths, *Synchronization: A Universal Concept in Nonlinear Sciences* (Cambridge University Press, Cambridge, 2001).
[2] S. H. Strogatz, Physica D **143**, 1 (2000).
[3] J. A. Acebrón, L. L. Bonilla, C. J. Pérez Vicente, F. Ritort, and R. Spigler, Rev. Mod. Phys. **77**, 137 (2005).
[4] F. Dörfler and F. Bullo, Automatica **50**, 1539 (2014).
[5] F. A. Rodrigues, T. K. D. Peron, P. Ji, and J. Kurths, Phys. Rep. **610**, 1 (2016).
[6] Y. Kuramoto, *Lecture Notes in Physics, International Symposium on Mathematical Problems in Theoretical Physics*, edited by H. Araki (Springer-Verlag, New York, 1975), Vol. 39; Y. Kuramoto, *Chemical Oscillations, Waves and Turbulence* (Springer-Verlag, New York, 1984), Vol. 39.
[7] E. Ott and T. M. Antonsen, Chaos **18**, 037113 (2008).
[8] E. Ott and T. M. Antonsen, Chaos **19**, 023117 (2009).
[9] E. A. Martens, E. Barreto, S. H. Strogatz, E. Ott, P. So, and T. M. Antonsen, Phys. Rev. E **79**, 026204 (2009).
[10] E. Ott, B. R. Hunt, and T. M. Antonsen, Chaos **21**, 025112 (2011).
[11] A. Pikovsky and M. Rosenblum, Physica D **240**, 872 (2011).
[12] H. Hong and S. H. Strogatz, Phys. Rev. Lett. **106**, 054102 (2011).
[13] M. Wolfrum, S. V. Gurevich, and O. E. Omel'chenko, Nonlinearity **29**, 257 (2016).
[14] T. B. Luke, E. Barreto, and P. So, Neural Comput. **25**, 3207 (2013).
[15] P. So, T. B. Luke, and E. Barreto, Physica D **267**, 16 (2014).
[16] T. B. Luke, E. Barreto, and P. So, Front. Comput. Neurosci. **8**, 1 (2014).
[17] C. R. Laing, Phys. Rev. E **90**, 010901 (2014).
[18] C. R. Laing, SIAM J. Appl. Dynam. Syst. **14**, 1899 (2015).
[19] D. Pazó and E. Montbrió, Phys. Rev. X **4**, 011009 (2014).
[20] R. Gallego, E. Montbrió, and D. Pazó, Phys. Rev. E **96**, 042208 (2017).

[21] E. Montbrió, D. Pazó, and A. Roxin, Phys. Rev. X **5**, 021028 (2015).
[22] I. Ratas and K. Pyragas, Phys. Rev. E **94**, 032215 (2016).
[23] D. Pazó and E. Montbrió, Phys. Rev. Lett. **116**, 238101 (2016).
[24] I. Ratas and K. Pyragas, Phys. Rev. E **96**, 042212 (2017).
[25] J. M. Esnaola-Acebes, A. Roxin, D. Avitabile, and E. Montbrió, Phys. Rev. E **96**, 052407 (2017).
[26] F. Atay and A. Hutt, SIAM J. Appl. Dynam. Syst. **5**, 670 (2006).
[27] A. Hutt and L. Zhang, J. Math. Neurosci. **3**, 9 (2013).
[28] W. S. Lee, E. Ott, and T. M. Antonsen, Phys. Rev. Lett. **103**, 044101 (2009).
[29] H. Daido and K. Nakanishi, Phys. Rev. Lett. **93**, 104101 (2004).
[30] D. Pazó and E. Montbrió, Phys. Rev. E **73**, 055202 (2006).
[31] H. Daido and K. Nakanishi, Phys. Rev. E **75**, 056206 (2007).
[32] H. Daido, EPL **84**, 10002 (2008).
[33] H. Daido, A. Kasama, and K. Nishio, Phys. Rev. E **88**, 052907 (2013).
[34] G. Tanaka, K. Morino, H. Daido, and K. Aihara, Phys. Rev. E **89**, 052906 (2014).
[35] B. Thakur, D. Sharma, and A. Sen, Phys. Rev. E **90**, 042904 (2014).
[36] B. Rahman, K. B. Blyuss, and Y. N. Kyrychko, Phys. Rev. E **96**, 032203 (2017).
[37] A. Dhooge, W. Govaerts, and Y. A. Kuznetsov, ACM Trans. Math. Softw. **29**, 141 (2003).
[38] F. Devalle, A. Roxin, and E. Montbrió, PLoS Comput. Biol. **13**, e1005881 (2017).
[39] A. Destexhe and T. J. Sejnowski, Biol. Cybern. **101**, 1 (2009).